

Structural and transport properties of highly Ru-deficient SrRu_{0.7}O₃ thin films prepared by molecular beam epitaxy: comparison with stoichiometric SrRuO₃

Yuki K. Wakabayashi,^{1,*†} Shingo Kaneta-Takada,^{1,2,*} Yoshiharu Krockenberger,¹ Kosuke Takiguchi,^{1,2} Shinobu Ohya,^{2,3} Masaaki Tanaka,^{2,4} Yoshitaka Taniyasu,¹ and Hideki Yamamoto¹

¹*NTT Basic Research Laboratories, NTT Corporation, Atsugi, Kanagawa 243-0198, Japan*

²*Department of Electrical Engineering and Information Systems, The University of Tokyo, Bunkyo, Tokyo 113-8656, Japan*

³*Institute of Engineering Innovation, The University of Tokyo, Bunkyo, Tokyo 113-8656, Japan*

⁴*Center for Spintronics Research Network (CSRN), The University of Tokyo, Bunkyo, Tokyo 113-8656, Japan*

*These authors contributed equally to this work.

†Author to whom correspondence should be addressed:
yuuki.wakabayashi.we@hco.ntt.co.jp

Abstract

We investigate structural and transport properties of highly Ru-deficient SrRu_{0.7}O₃ thin films prepared by molecular beam epitaxy on (001) SrTiO₃ substrates. To distinguish the influence of the two types of disorders in the films—Ru vacancies within lattices and disorders near the interface—SrRu_{0.7}O₃ thin films with various thicknesses ($t = 1\text{--}60$ nm) were prepared. It was found that the influence of the former dominates the electrical and magnetic properties when $t \geq 5\text{--}10$ nm, while that of the latter does when $t \leq 5\text{--}10$ nm. Structural characterizations revealed that the crystallinity, in terms of the Sr and O sublattices, of SrRu_{0.7}O₃ thin films, is as high as that of the ultrahigh-quality SrRuO₃ ones. The Curie temperature (T_C) analysis elucidated that SrRu_{0.7}O₃ ($T_C \approx 140$ K) is a material distinct from SrRuO₃ ($T_C \approx 150$ K). Despite the large Ru deficiency ($\sim 30\%$), the SrRu_{0.7}O₃ films showed metallic conduction when $t \geq 5$ nm. In high-field magnetoresistance measurements, the fascinating phenomenon of Weyl fermion transport was not observed for the SrRu_{0.7}O₃ thin films irrespective of thickness, which is in contrast to the stoichiometric SrRuO₃ films. The (magneto)transport properties suggest that a picture of carrier scattering due to the Ru vacancies is appropriate for SrRu_{0.7}O₃, and also that proper stoichiometry control is a prerequisite to utilizing the full potential of SrRuO₃ as a magnetic Weyl semimetal and two-dimensional spin-polarized system. Nevertheless, the large tolerance in Ru composition ($\sim 30\%$) to metallic conduction is advantageous for some practical applications where SrRu_{1-x}O₃ is exploited as an epitaxial conducting layer.

The itinerant $4d$ ferromagnetic perovskite SrRuO_3 has attracted strong attention because of the unique nature of its ferromagnetism, metallicity, chemical stability, and compatibility with other perovskite-structured oxides.^{1–17} It has been widely used in oxide electronics and spintronics as an epitaxial conducting layer.⁸ Recently, interest in SrRuO_3 has been further boosted by the observation of Weyl fermions^{18,19} and the realization of two-dimensional ferromagnetism in electrically conducting layers of one-unit-cell thickness embedded in $[(\text{SrRuO}_3)_1/(\text{SrTiO}_3)_n]$ heterostructures.^{20,21} These intriguing phenomena are observed only in samples of exceptionally high quality;^{18,20} specifically, those with a high residual resistivity ratio (RRR), which is known to be a good indicator of the purity of metallic systems.^{8,11,18}

To apply the magnetic Weyl semimetal state and two-dimensional ferromagnetism in SrRuO_3 -based heterostructures to newly proposed spintronic devices²² and topoelectrical circuits,^{23,24} we must be able to control the interfaces between the SrRuO_3 and other layers. A promising approach to gain insight into the interfaces is to investigate thickness-dependent (magneto)transport properties of SrRuO_3 films, especially down to the nanometer scale. This is because the contribution of interface-driven disorders on the transport properties varies with thickness.¹⁹ Several studies on such ultra-thin SrRuO_3 films, including our previous ones, have demonstrated higher resistivity and a lower Curie temperature (T_C) with decreasing film thickness.^{8,25–29} When SrRuO_3 film thickness is below 2 nm, neither residual resistivity (thus, the RRR) nor T_C could be well-defined because an insulating and nonferromagnetic state emerges.^{25–29} The only exception is atomically thin SrRuO_3 (0.4 nm) layers embedded in $[(\text{SrRuO}_3)_1/(\text{SrTiO}_3)_n]$ heterostructures that show ferromagnetic and conducting behavior.^{20,21} On the other hand, our recent study showed that the threshold RRR to observe transport phenomena stemming from the Weyl fermions is ~ 20 , which corresponds to thickness $t \geq 10$ nm for stoichiometric films reasonably free from Ru vacancies.¹⁹

Here, there are two possible origins of low RRR values in SrRuO_3 . One is poor crystallinity due to high impurity density and/or structural disorders, which is generally seen in low-quality samples.^{8,11,12,30,31} The other one is Ru vacancies, which is rather specific to SrRuO_3 .^{8,11} It is therefore required to distinguish between these two possibilities in order to improve the quality of SrRuO_3 samples. Stringent stoichiometry control during the film growth is required if the Ru vacancies dominate disorder. However, those two sources have sometimes been mixed up, and there is a dearth of knowledge on the influence of off-stoichiometry on the transport, especially quantum transport properties.

In this study, we investigated the (magneto)transport properties of epitaxial SrRuO_3 films with various thicknesses grown under highly Ru-deficient conditions, and compared the results with those for stoichiometric films, which we have already reported.^{18,19} Using molecular beam epitaxy (MBE), we can vary the ratio of the Sr and Ru beam fluxes supplied *ad arbitrium* during the growth and thus design and prepare such highly Ru-deficient $\text{SrRu}_{1-x}\text{O}_3$ thin films whose crystallinity, in terms of the Sr and O sub-lattices, is as high as that of stoichiometric (SrRuO_3) thin films. Similar composition controls are almost impossible with other thin-film growth techniques such as pulsed-laser deposition and sputtering, where the preparation of off-stoichiometric targets is a prerequisite. The chemical composition of a Ru-deficient film with thickness $t = 60$ nm was determined using energy dispersive X-ray spectroscopy (EDS)

measurements. Complementary information was obtained by X-ray photoelectron spectroscopy (XPS). For comparison, the EDS and XPS measurements were also carried out for a stoichiometric film with identical thickness.

Ru-deficient $\text{SrRu}_{1-x}\text{O}_3$ films with thickness t ranging from 1 to 60 nm were grown on (001) SrTiO_3 substrates in a custom-designed MBE setup equipped with multiple e-beam evaporators for Sr and Ru.^{18, 33} For comparison, a 60-nm-thick stoichiometric SrRuO_3 film was also prepared. Detailed information about our MBE setup and preparation of the substrates are described elsewhere.^{34–36} Oxidation during the growth was carried out with a mixture of ozone (O_3) and O_2 gas ($\sim 15\% \text{O}_3 + 85\% \text{O}_2$), which was introduced through an alumina nozzle pointed at the substrate at a flow rate of ~ 2 sccm. The growth temperature was fixed at 772°C for all the films.

We precisely controlled the elemental fluxes, even for elements with high melting points, e.g., Ru (2250°C), by monitoring the flux rates with an electron-impact-emission-spectroscopy sensor, which were fed back to the power supplies for the e-beam evaporators. The Ru flux rates were set at 0.190 and 0.365 $\text{\AA}/\text{s}$ for the growth of the Ru-deficient and stoichiometric films, respectively, while the Sr flux was kept at 0.98 $\text{\AA}/\text{s}$. The growth rate of 1.05 $\text{\AA}/\text{s}$ was deduced from the thickness calibration of a thick (60 nm) SrRuO_3 film using cross-sectional scanning transmission electron microscopy (STEM). This growth rate agrees very well with that (1.08 $\text{\AA}/\text{s}$) estimated from the flux rate of Sr, confirming the accuracy of the film thickness. This also indicates that the sticking coefficient of Sr can be deemed to be unity. In contrast, it is known that supplied Ru partially re-evaporates from the growth surface through the formation of volatile species such as RuO_4 and RuO_3 under oxidizing atmosphere,^{10,11} especially when excessive Ru is supplied; hence, one needs to grow films under a Ru-rich condition to form stoichiometric ones. The supplied Ru rates of 0.190 $\text{\AA}/\text{s}$ for Ru-deficient and 0.365 $\text{\AA}/\text{s}$ for stoichiometric films correspond to the Ru/Sr flux ratios of 0.80 (Ru-poor) and 1.54 (Ru-rich), respectively.

To determine the Ru/Sr composition ratios in the grown films, the 60-nm-thick films prepared under the Ru-poor and Ru-rich conditions were measured by EDS using a Bruker Quantax-400 EDS spectrometer [Fig. 1(a)]. The energy of the incident electron beam was 5 keV, and the probing area was $85 \times 115 \mu\text{m}^2$. Only the Sr, Ru, and O peaks are observed, indicating that the signals are exclusively from the films and the contribution from the SrTiO_3 substrates is negligible. We estimated the chemical compositions of the films using the conventional ZAF matrix correction routine built into the Bruker Esprit software,^{37,38} where Z, A, and F represent atomic number, absorption, and fluorescence corrections, respectively. The results indicate that the Ru/Sr ratios in the films grown under the Ru-poor and Ru-rich conditions are 0.71 and 1.03, respectively. The Ru/Sr ratio of 0.71 in the Ru-deficient film seems to be reasonable considering the upper limit set by the supplied Ru/Sr flux ratio is 0.80. On the other hand, the film grown under the Ru-rich condition turned out to be stoichiometric within the accuracy of EDS. It is possible that O sites are also vacant to some extent in the Ru-deficient films. Although quantitative estimation of oxygen content by EDS is elusive, a less intense O peak for the Ru-deficient film than the stoichiometric one [Fig. 1(a)] supports this possibility. Under the naive assumption that the O content is proportional to the peak intensity and that the stoichiometric film has a composition formula of SrRuO_3 , the Ru-deficient film is expressed as $\text{SrRu}_{0.71}\text{O}_{2.87}$. When the chemical formula of the Ru-deficient film is $\text{SrRu}_{0.7}\text{O}_{2.9}$ or $\text{SrRu}_{0.7}\text{O}_3$, the average valence of Ru is evaluated to be

+5.4 (Ru^{5.4+}) or +5.7 (Ru^{5.7+}), respectively, which is much higher than that (+4) in stoichiometric SrRuO₃ (Ru⁴⁺). The existence of such a high valence state is suggested by the chemical shift in the Ru 3*p*_{3/2} XPS spectra [Fig. 1(b)].³⁹⁻⁴² the Ru 3*p*_{3/2} level has slightly higher binding energy in SrRu_{0.7}O₃ (463.7 eV) than in SrRuO₃ (463.4 eV). The lower peak intensity in the XPS spectra for the SrRu_{0.7}O₃ film is also, at least qualitatively, consistent with the Ru/Sr ratio analysis by EDX. Those XPS measurements were performed with an ULVAC-PHI Model XPS5700 with a monochromatized Al K α (1486.6 eV) source operated at 200 W. Hereafter, the Ru-deficient films are denoted by SrRu_{0.7}O₃ because our main interest is the Ru-deficiencies and because reliable estimation of the O content by EDX or XPS is impossible.

Figure 2(a) shows the RHEED patterns of the Ru-deficient SrRu_{0.7}O₃ surfaces for various thicknesses *t*. Every film shows sharp streaky patterns, indicating that the growth of the SrRu_{0.7}O₃ film proceeded in a two-dimensional layer-by-layer manner. Figure 2(b) shows cross-sectional high-angle annular dark-field scanning transmission electron microscopy (HAADF-STEM) images of a Ru-deficient film with *t* = 60 nm. The SrRu_{0.7}O₃ film was grown epitaxially on a (001) SrTiO₃ substrate with an abrupt substrate/film interface, as expected from the RHEED patterns. Unexpectedly, these RHEED patterns and STEM images for the Ru-deficient SrRu_{0.7}O₃ films are almost identical to those for the stoichiometric SrRuO₃ films reported previously,¹⁹ even though around 30% of Ru sites are missing. This indicates that Ru vacancies are not line or plane defects but point defects, which are insensitive to RHEED and cross-sectional STEM measurements when they are randomly distributed. The caveat here is that SrRu_{0.7}O₃ is indistinguishable from SrRuO₃ in HAADF-STEM, which has atomic resolution as well as elemental discrimination capability. In Fig. 2(c), θ -2 θ X-ray diffraction (XRD) patterns are compared between the SrRu_{0.7}O₃ and SrRuO₃ films with a common thickness of 60 nm. The sharpness, intensity, and relative intensity of the peaks [not shown in Fig. 2(c)] are essentially identical between the two XRD patterns. In addition, Laue fringes around the (004) peaks (peaks are indexed for pseudocubic lattices) are clearly observed in both patterns. These results indicate that the overall crystallinity of the SrRu_{0.7}O₃ film is as high as that of the SrRuO₃ film. The out-of-plane lattice constant estimated by the Nelson-Riley extrapolation method is 3.951 Å for the Ru-deficient SrRu_{0.7}O₃ film, which is slightly larger than the value (3.949 Å) for the stoichiometric SrRuO₃ film.¹⁹ This is consistent with previous reports claiming that the existence of Ru vacancies increases the out-of-plane lattice constant of SrRuO₃ films on SrTiO₃ substrates.^{11,43} While preparation of bulk single crystals with highly Ru-deficient compositions (~30%) remains to be done, we speculate that epitaxial stabilization may have fostered the formation of the perovskite-structured SrRu_{0.7}O₃ films whose crystallinity is comparably high to that of stoichiometric ones. Altogether, structural characterizations by RHEED, STEM, and XRD provide almost identical results for SrRu_{0.7}O₃ and SrRuO₃, except for the subtle change in the lattice parameter.

We subsequently investigated the (magneto)transport properties of the Ru-deficient SrRu_{0.7}O₃ films, which were measured by a standard four-point-probe method with Ag electrodes deposited on the film surfaces without any additional processing. The distance between the two voltage electrodes was 2 mm. To begin with, the temperature dependence of the longitudinal resistivity ρ_{xx} of the SrRu_{0.7}O₃ films with various thickness *t* is shown in Fig. 3(a). No external magnetic field was applied. The ρ_{xx} values of the films with *t* = 5 – 60 nm decrease with decreasing temperature *T*, indicating that

these films are metallic in the whole temperature range measured. The $\rho_{xx}(T)$ curves converge in the thickness range of 10–60 nm— $\rho_{xx}(300\text{ K}) \approx 180\ \mu\Omega\cdot\text{cm}$ and $\rho_{xx}(2\text{ K}) \approx 30\ \mu\Omega\cdot\text{cm}$, while the curve for the 5-nm-thick film shows an almost parallel shift to higher ρ_{xx} by a few tens of $\mu\Omega\cdot\text{cm}$. These transport properties of the $\text{SrRu}_{0.7}\text{O}_3$ films with $t = 10\text{--}60$ nm are in stark contrast to the stoichiometric SrRuO_3 case. In Fig. 3(b), t -dependent residual resistivity $\rho_{\text{Res}} [\rho_{xx}(2\text{ K})]$ for the $\text{SrRu}_{0.7}\text{O}_3$ and SrRuO_3 films is shown. The data for the stoichiometric films are from our previous report.¹⁹ The ρ_{Res} of the Ru-deficient films stays almost constant for $t = 10\text{--}60$ nm, whereas it gradually but monotonically increases from 2.0 to 7.5 $\mu\Omega\cdot\text{cm}$ with decreasing thickness from 60 to 10 nm in the stoichiometric ones. Furthermore, ρ_{Res} is higher in $\text{SrRu}_{0.7}\text{O}_3$ than in SrRuO_3 at each thickness. These results indicate the transport properties of the $\text{SrRu}_{0.7}\text{O}_3$ films are dominated by the scattering due to the Ru vacancies, rather than by interface-driven disorders, especially when $t \geq 10$ nm. In the stoichiometric films, an abrupt increase in ρ_{Res} occurs in the thickness range of $t \leq 10$ nm, suggesting that carrier scattering at the interface-driven disorders plays a dominant role. Note that we consider interface-driven disorders whose types are insensitive to STEM observations. It is also noteworthy that SrRuO_3 might have been regarded as a bad metal based on experimental results for Ru-deficient specimens like $\text{SrRu}_{0.7}\text{O}_3$, since ten-times larger ρ_{Res} leads to one order of magnitude smaller mean free path estimation.⁸

In Fig. 3(a), $\rho_{xx}(T)$ curves for the thinner films are also plotted. The ρ_{xx} values of the 2-nm-thick film decrease with decreasing temperature from 300 K down to $T_{\rho\text{min}}$, at which the ρ_{xx} becomes minimum, but for $T < T_{\rho\text{min}}$, ρ_{xx} increases with decreasing temperature. This insulating behavior ($d\rho_{xx}/dT < 0$) possibly stems from the weak-localization in the low-temperature range,^{20,25–29} which is enhanced due to structural disorders, including lattice point defects (Ru vacancies) and some boundaries.⁴⁴ With a further decrease in t down to 1 nm [inset in Fig. 3(a)], the ρ_{xx} values become three to four orders of magnitude larger than those of the other films, and $d\rho_{xx}/dT$ is negative for the whole measurement temperature range (2–300 K); that is, the influence of interface-driven disorder prevails against Ru deficiencies in ultrathin films ($t \leq 2$ nm). Similar thickness-dependent insulating behaviors have been reported by many other groups.^{20,25–29} In most of those studies, insulating behavior starts to appear when the film thickness is 2–4 nm,^{25–28} implying that those films are subject to interface-driven disorders and possibly also to the cation off-stoichiometry problem. This interpretation seems reasonable as the high-crystalline-quality stoichiometric thin film with $t = 2$ nm was metallic in our previous study.¹⁹ In Fig. 3(c), we compare the t dependence of the RRR [$= \rho_{xx}(300\text{ K})/\rho_{xx}(2\text{ K})$] between the $\text{SrRu}_{0.7}\text{O}_3$ and SrRuO_3 films with $t \geq 2$ nm. The thickness dependence is substantially smaller in $\text{SrRu}_{0.7}\text{O}_3$ than in SrRuO_3 , which is consistent with our consideration that the transport process is mainly limited by scattering within a lattice (Ru vacancies) for $\text{SrRu}_{0.7}\text{O}_3$ and interface-driven disorders for SrRuO_3 .

When $t \geq 5$ nm, the $\rho_{xx}(T)$ curves show clear kinks at around 140 K [arrow in Fig. 3(a)], at which the ferromagnetic transition occurs and spin-dependent scattering is suppressed.⁸ To highlight the ferromagnetic transition, we plot the derivative resistivity $d\rho_{xx}/dT$ as a function of T [Fig. 3(d)]. Here, we define T_C as the temperature at which the $d\rho_{xx}/dT$ or $\rho_{xx}(T)$ curves show a clear peak or kink [solid arrows in Fig. 3(d)], respectively. We note that, in general, the T_C determined from $d\rho_{xx}/dT$ is a few K lower than the values measured from the temperature dependence of the magnetization.²⁷ Apart from a small hump at higher temperatures observed for the films with $t = 40$ and 60 nm, $d\rho_{xx}/dT$ curves

and peak positions are essentially identical in the films with $t = 10\text{--}60$ nm, which exhibit a common T_C of 140 K. The t dependence of T_C in Fig. 3(e), in which the $T_C(t)$ curves for $\text{SrRu}_{0.7}\text{O}_3$ and SrRuO_3 show a parallel shift, indicates that the highly Ru-deficient $\text{SrRu}_{0.7}\text{O}_3$ films inherently have a distinct T_C of ≈ 140 K in the absence of interface-driven disorders ($t = 10\text{--}60$ nm), and that their T_C values are 10 K lower than that of the stoichiometric SrRuO_3 films. In other words, the influence of the 30% Ru-deficiency on the magnetic ordering temperature is as small as 10 K. For $t < 10$ nm, T_C sharply decreases (down to ≈ 100 K) with decreasing thickness irrespective of $\text{SrRu}_{0.7}\text{O}_3$ or SrRuO_3 , indicating that the influence of the interface-driven disorders on the reduction of the exchange interaction (and thus the decrease in T_C) is larger than that of the Ru-deficiencies.

As mentioned above, the RRR of the $\text{SrRu}_{0.7}\text{O}_3$ films takes an almost constant value of about 5 when $t = 10\text{--}60$ nm and decreases to a value of a little larger than unity for $t = 2$ nm [Fig. 3(c)] (here, the residual resistivity for the 2-nm-thick film is estimated based on the ρ_{\min} value). On the other hand, T_C stays almost constant (≈ 140 K) for $t = 10\text{--}60$ nm and sharply decreases with decreasing t from 10 to 2 nm. As a result, T_C sharply varies as a function of RRR for the Ru-deficient $\text{SrRu}_{0.7}\text{O}_3$ films [Fig. 3(f)]. This trend for the $\text{SrRu}_{0.7}\text{O}_3$ films is similar to what is derived for stoichiometric SrRuO_3 films.^{18,19} For the stoichiometric SrRuO_3 films, the RRR values varied in a much wider range; ultrahigh-quality SrRuO_3 films with $t = 63$ nm showed a very high RRR value of larger than 84.¹⁹ The intermediate data points are obtained during the growth condition optimization processes and/or by varying the thickness of the SrRuO_3 films.^{18,19} Accordingly, different RRR values have various origins, including Ru and/or O vacancies, orthorhombic domains, and interface-driven disorders.^{8,30,31} Nevertheless, the universal trend in the T_C vs. RRR plots indicates that T_C is rather insensitive to the RRR when it is ≥ 20 , irrespective of the origins of the lower RRR, whereas T_C is very sensitive to the RRR when it is < 20 in the material system of $\text{SrRu}_{1-x}\text{O}_3$ including $x = 0$. The threshold value of around 20 coincides with what is required to observe transport phenomena specific to the magnetic Weyl semimetal state.^{18,19}

We also performed magnetotransport measurements on the Ru-deficient $\text{SrRu}_{0.7}\text{O}_3$ films by the standard four-point-probe method. In Fig. 4(a), we show the t dependence of the magnetoresistance (MR) $[(\rho_{xx}(B) - \rho_{xx}(0\text{ T})) / \rho_{xx}(0\text{ T})]$, where the magnetic field B is applied in the out-of-plane [001] direction of the SrTiO_3 substrate at 2 K. For comparison, in Ref. [19], the signatures of quantum transport of the Weyl fermions, e.g., the unsaturated linear positive MR accompanied by quantum oscillations having a π Berry phase, are observed in the stoichiometric SrRuO_3 films with $t \geq 10$ nm. In the Ru-deficient $\text{SrRu}_{0.7}\text{O}_3$ films, however, the MR at high magnetic fields is negative and the SdH oscillations are not observed for any films, irrespective of the thickness [Fig. 4(a)]. From the results shown in Fig. 4(a), we extracted the thickness dependence of the MR ratios for the highest applied magnetic field $[(\rho_{xx}(9\text{ T}) - \rho_{xx}(0\text{ T})) / \rho_{xx}(0\text{ T})]$ at 2 K [Fig. 4(b)]. The MR ratio of the $\text{SrRu}_{0.7}\text{O}_3$ films increases with increasing thickness and saturates to the MR = 0% line. In contrast to the stoichiometric SrRuO_3 case,¹⁹ which is also plotted in Fig. 4(b), the thickness dependence is weak, and the values of the MR ratio never exceed zero. Since the positive MR comes from the Weyl fermions in SrRuO_3 ,^{18,19} the magnetic Weyl semimetal state is not realized in the $\text{SrRu}_{0.7}\text{O}_3$ even when $t = 60$ nm; the Weyl semimetal state is observed only in the stoichiometric SrRuO_3 films with $t \geq 10$ nm. These results indicate two scenarios: 1) the scattering at the Ru vacancies in the

SrRu_{0.7}O₃ films hinders the emergence of quantum transport phenomena stemming from the Weyl fermions, or 2) the magnetic Weyl semimetal state itself is not realized in SrRu_{0.7}O₃ near the Fermi level *per se* due to the difference in electronic structure. The MR vs. RRR plot of the Ru-deficient SrRu_{0.7}O₃ films seems to fall within the trend derived from the stoichiometric SrRuO₃ films [Fig. 4(c)]. For SrRuO₃, the MR ratio increases with increasing RRR and eventually has positive values when the RRR is larger than 20, meaning that the Weyl fermions dominate the transport properties when the SrRuO₃ film has less defects.

In Fig. 4(a), for the SrRu_{0.7}O₃ films with $t \leq 10$ nm, anisotropic magnetoresistance (AMR),⁴⁵ which is proportional to the relative angle between the electric current and the magnetization, is clearly observed below 3 T at 2 K. In SrRuO₃, the AMR peak position corresponds to the coercive field H_c .¹⁸ On the other hand, SrRu_{0.7}O₃ films with $t \geq 20$ nm show hysteresis in the MR above H_c of the 10-nm-thick film (~ 1 T). Such features in the MR hysteresis suggest the existence of two different magnetic components in the SrRu_{0.7}O₃ films. The two component scenario is also supported by hump structures observed in the $d\rho_{xx}/dT$ vs. temperature curves for the films with $t = 40$ and 60 nm. The hump structures are discernible at around 150 K [dashed arrows in Fig. 3(d)], indicating the existence of two distinct T_C values,⁴⁶ possibly due to inhomogeneous distribution of the Ru vacancies.

In summary, we investigated the structural and transport properties of the highly Ru-deficient SrRu_{0.7}O₃ thin films prepared by MBE on (001) SrTiO₃ substrates, and compared the results to those for stoichiometric SrRuO₃ thin films. To distinguish the influence of the two types of disorders—Ru vacancies within lattices and interface-driven disorders—SrRu_{0.7}O₃ thin films with various thicknesses ($t = 1 - 60$ nm) were prepared. It turned out that the influence of the former dominates the electrical and magnetic properties when $t \geq 5 - 10$ nm, while that of the latter does for $t \leq 5 - 10$ nm. Emphasis should be placed on the fact that the crystalline quality of the SrRu_{0.7}O₃ films is as high as that of ultrahigh-quality SrRuO₃ thin films, and that structural characterizations by RHEED, STEM, and XRD cannot distinguish the difference between SrRu_{0.7}O₃ and SrRuO₃ except for a subtle change in the lattice parameter. In view of the Curie temperature T_C , SrRu_{0.7}O₃ ($T_C \approx 140$ K) can be regarded as a material distinct from SrRuO₃ ($T_C \approx 150$ K). From the viewpoint of the transport properties, SrRu_{0.7}O₃ can be understood to be highly Ru-deficient SrRuO₃, where Ru vacancies serve as charge carrier scatter centers. Even if 30% of Ru sites are vacant, metallic conduction ($d\rho_{xx}/dT > 0$) is preserved for the films with $t \geq 5$ nm. This large tolerance in Ru composition is advantageous for some practical applications as an epitaxial conducting layer. At present, the ultrathin films ($t < 10$ nm) are inevitably subject to interface-driven disorders, irrespective of SrRu_{0.7}O₃ or SrRuO₃. Adopting different substrates that have less lattice mismatch may help to overcome the interface-driven disorder problem.

AUTHORS' CONTRIBUTIONS

Y.K.W. conceived the idea, designed the experiments, and led the project. Y.K.W. and Y.K. grew the samples. Y.K.W. and S.K.T. carried out the sample characterizations. S.K.T. and Y.K.W. carried out the transport measurements and analyzed the data. All authors contributed to the discussion of the data. Y.K.W. and S.K.T. co-wrote the paper with input from all authors.

DATA AVAILABILITY

The data that support the findings of this study are available from the corresponding author upon reasonable request.

References

- ¹ J. J. Randall and R. Ward, *J. Am. Chem. Soc.* **81**, 2629 (1959).
- ² J. M. Longo, P. M. Raccach, and J. B. Goodenough, *J. Appl. Phys.* **39**, 1327 (1968).
- ³ R. J. Bouchard and J. L. Gillson, *Mater. Res. Bull.* **7**, 873 (1972).
- ⁴ L. Klein and J. S. Dodge, C. H. Ahn, J. W. Reiner, L. Mieville, T. H. Geballe, M. R. Beasley, and A. Kapitulnik, *J. Phys. Condens. Matter* **8**, 10111, (1996).
- ⁵ C. B. Eom, R. J. Cava, R. M. Fleming, J. M. Phillips, R. B. van Dover, J. H. Marshall, J. W. P. Hsu, J. J. Krajewski, and W. F. Peck, Jr., *Science* **258**, 1766, (1992).
- ⁶ X. D. Wu, S. R. Foltyn, R. C. Dye, Y. Coulter, and R. E. Muenchausen, *Appl. Phys. Lett.* **62**, 2434 (1993).
- ⁷ M. Izumi, K. Nakazawa, Y. Bando, Y. Yoneda, and H. Terauchi, *J. Phys. Soc. Jpn.* **66**, 3893 (1997).
- ⁸ G. Koster, L. Klein, W. Siemons, G. Rijnders, J. S. Dodge, C.-B. Eom, D. H. A. Blank, M. R. Beasley, *Rev. Mod. Phys.* **84**, 253 (2012).
- ⁹ D. Kan, M. Mizumaki, T. Nishimura, and Y. Shimakawa, *Phys. Rev. B*, **94**, 214420, (2016).
- ¹⁰ H. P. Nair, Y. Liu, J. P. Ruf, N. J. Schreiber, S.-L. Shang, D. J. Baek, B. H. Goodge, L. F. Kourkoutis, Z.-K. Liu, K. M. Shen, and D. G. Schlom, *APL Mater.* **6**, 046101 (2018).
- ¹¹ W. Siemons, G. Koster, A. Vailionis, H. Yamamoto, D. H. A. Blank, and M. R. Beasley, *Phys. Rev. B* **76**, 075126 (2007).
- ¹² J. Thompson, J. Nichols, S. Lee, S. Ryee, J. H. Gruenewald, J. G. Connell, M. Souri, J. M. Johnson, J. Hwang, M. J. Han, H. N. Lee, D.-W. Kim, and S. S. A. Seo, *Appl. Phys. Lett.* **109**, 161902 (2016).
- ¹³ D. E. Shai, C. Adamo, D. W. Shen, C. M. Brooks, J. W. Harter, E. J. Monkman, B. Burganov, D. G. Schlom, and K.M. Shen, *Phys. Rev. Lett.* **110**, 087004 (2013).
- ¹⁴ A. P. Mackenzie, J. W. Reiner, A. W. Tyler, L. M. Galvin, S. R. Julian, M. R. Beasley, T. H. Geballe, and A. Kapitulnik, *Phys. Rev. B* **58**, R13318 (1998).
- ¹⁵ D. C. Worledge and T. H. Geballe, *Phys. Rev. Lett.* **85**, 5182 (2000).
- ¹⁶ K. S. Takahashi, A. Sawa, Y. Ishii, H. Akoh, M. Kawasaki, and Y. Tokura, *Phys. Rev. B* **67**, 094413 (2003).
- ¹⁷ Z. Li, S. Shen, Z. Tian, K. Hwangbo, M. Wang, Y. Wang, F. M. Bartram, L. He, Y. Lyu, Y. Dong, G. Wan, H. Li, N. Lu, J. Zang, H. Zhou, E. Arenholz, Q. He, L. Yang, W. Luo, and P. Yu, *Nat. Commun.* **11**, 184 (2020).
- ¹⁸ K. Takiguchi, Y. K. Wakabayashi, H. Irie, Y. Krockenberger, T. Otsuka, H. Sawada, S. A. Nikolaev, H. Das, M. Tanaka, Y. Taniyasu, and H. Yamamoto, *Nat. Commun.* **11**, 4969 (2020).
- ¹⁹ S. K. Takada, Y. K. Wakabayashi, Y. Krockenberger, S. Ohya, M. Tanaka, Y. Taniyasu, and H. Yamamoto, *arXiv:2011.03670*.
- ²⁰ H. Boschker, T. Harada, T. Asaba, R. Ashoori, A. V. Boris, H. Hilgenkamp, C. R. Hughes, M. E. Holtz, L. Li, D. A. Muller, H. Nair, P. Reith, X. R. Wang, D. G. Schlom,

- A. Soukiassian, and J. Mannhart, *Phys. Rev. X* **9**, 011027 (2019).
- ²¹ Z. Cui, A. J. Grutter, H. Zhou, H. Cao, Y. Dong, D. A. Gilbert, J. Wang, Y.-S. Liu, J. Ma, Z. Hu, J. Guo, J. Xia, B. J. Kirby, P. Shafer, E. Arenholz, H. Chen, X. Zhai, and Y. Lu, *Sci. Adv.* **6**, eaay0114 (2020).
- ²² Y. Araki and K. Nomura, *Phys. Rev. Appl.* **10**, 014007 (2018).
- ²³ C. H. Lee, S. Imhof, C. Berger, F. Bayer, J. Brehm, L. W. Molenkamp, T. Kiessling, and R. Thomale, *Commun. Phys.* **1**, 39 (2018).
- ²⁴ S. M. Rafi-Ul-Islam, Z. B. Siu, and M. B. A. Jalil, *Commun. Phys.* **1**, 72 (2020).
- ²⁵ D. Toyota, I. Ohkubo, H. Kumigashira, M. Oshima, T. Ohnishi, M. Lippmaa, M. Takizawa, A. Fujimori, K. Ono, M. Kawasaki, and H. Koinuma, *Appl. Phys. Lett.* **87**, 162508 (2005).
- ²⁶ X. Shen, X. Qiu, D. Su, S. Zhou, A. Li, and D. Wu, *J. Appl. Phys.* **117**, 015307 (2015).
- ²⁷ A. Rastogi, M. Brahlek, J. M. Ok, Z. Liao, C. Sohn, S. Feldman, and H. N. Lee, *APL Mater.* **7**, 091106 (2019).
- ²⁸ J. Xia, W. Siemons, G. Koster, M. R. Beasley, and A. Kapitulnik, *Phys. Rev. B* **79**, 140407(R) (2009).
- ²⁹ Y. J. Chang, C. H. Kim, S.-H. Phark, Y. S. Kim, J. Yu, and T. W. Noh, *Phys. Rev. Lett.* **103**, 057201 (2009).
- ³⁰ Q. Gan, R. A. Rao, and C. B. Eom, *Appl. Phys. Lett.* **70**, 1962 (1997).
- ³¹ J.C. Jiang, W. Tian, X. Pan, Q. Gan, C.B. Eom, *Mater. Sci. Eng. B* **56**, 152 (1998).
- ³² Y. K. Wakabayashi, T. Otsuka, Y. Taniyasu, H. Yamamoto, and H. Sawada, *Appl. Phys. Express* **11**, 112401 (2018).
- ³³ Y. K. Wakabayashi, T. Otsuka, Y. Krockenberger, H. Sawada, Y. Taniyasu, and H. Yamamoto, *APL Mater.* **7**, 101114 (2019).
- ³⁴ M. Naito and H. Sato, *Appl. Phys. Lett.* **67**, 2557 (1995).
- ³⁵ H. Yamamoto, Y. Krockenberger, and M. Naito, *J. Cryst. Growth* **378**, 184 (2013).
- ³⁶ Y. K. Wakabayashi, Y. Krockenberger, N. Tsujimoto, T. Boykin, S. Tsuneyuki, Y. Taniyasu, and H. Yamamoto, *Nat. Commun.* **10**, 535 (2019).
- ³⁷ D. E. Newbury and N. W. M. Ritchie, *J. Mater. Sci.* **50**, 493 (2015).
- ³⁸ P. A. Ferreira, P. R. Alonso, D. P. Quiros, E. Zelaya, G.H. Rubiolo, *Journal of Alloys and Compounds* **847**, 156372 (2020).
- ³⁹ R. Kotz, H. J. Lewerenz, and S. Stucki, *J. Electrochem. Soc.* **130**, 825 (1983).
- ⁴⁰ M. Takizawa, D. Toyota, H. Wadati, A. Chikamatsu, H. Kumigashira, A. Fujimori, M. Oshima, Z. Fang, M. Lippmaa, M. Kawasaki, and H. Koinuma, *Phys. Rev. B* **72**, 060404(R) (2005).
- ⁴¹ F. Yan, M.-O. Lai, L. Lu, and T.-J. Zhu, *J. Phys. Chem. C* **114**, 6994 (2010).
- ⁴² G. Berti, S. Sanna, C. Castellano, J. V. Duijn, R. R. Bustos, L. Bordonali, G. Bussetti, A. Calloni, F. Demartin, L. Duò, and A. Brambilla, *J. Phys. Chem. C* **120**, 11763 (2016).
- ⁴³ B. Dabrowski, O. Chmaissem, P. W. Klamut, S. Kolesnik, M. Maxwell, J. Mais, Y. Ito, B. D. Armstrong, J. D. Jorgensen, and S. Short, *Phys. Rev. B* **70**, 014423 (2004).
- ⁴⁴ G. Herranz, F. Sanchez, B. Martinez, J. Fontcuberta, M. V. Garcia-Cuenca, C. Ferrater, M. Varela, and P. Levy, *Eur. Phys. J. B* **40**, 439 (2004).
- ⁴⁵ D. B. Kacedon, R. A. Rao, and C. B. Eom, *Appl. Phys. Lett.* **71**, 1724 (1997).
- ⁴⁶ J. Lu, L. Si, X. Yao, C. Tian, J. Wang, Q. Zhang, Z. Lai, I. A. Malik, X. Liu, P. Jiang, K. Zhu, Y. Shi, Z. Luo, L. Gu, K. Held, W. Mi, Z. Zhong, C-W. Nan, and J. Zhang, *Phys. Rev. B* **101**, 214401 (2020).

Figures and figure captions

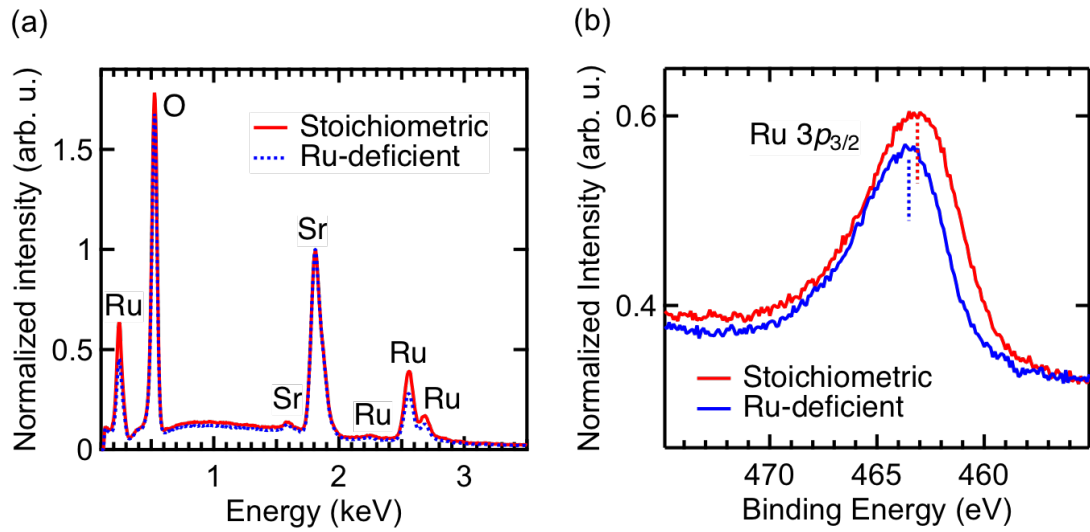


FIG. 1. (a) EDS spectra of the stoichiometric and Ru-deficient SrRuO_3 films with $t = 60$ nm, which were taken from a wide area ($85 \times 115 \mu\text{m}^2$) of the films. (b) Ru $3p_{3/2}$ XPS spectra of the stoichiometric and Ru-deficient SrRuO_3 films with $t = 60$ nm. Dashed lines indicate peak positions. The XPS spectra are normalized at the Sr $3d_{5/2}$ XPS peak intensities for easy comparison.

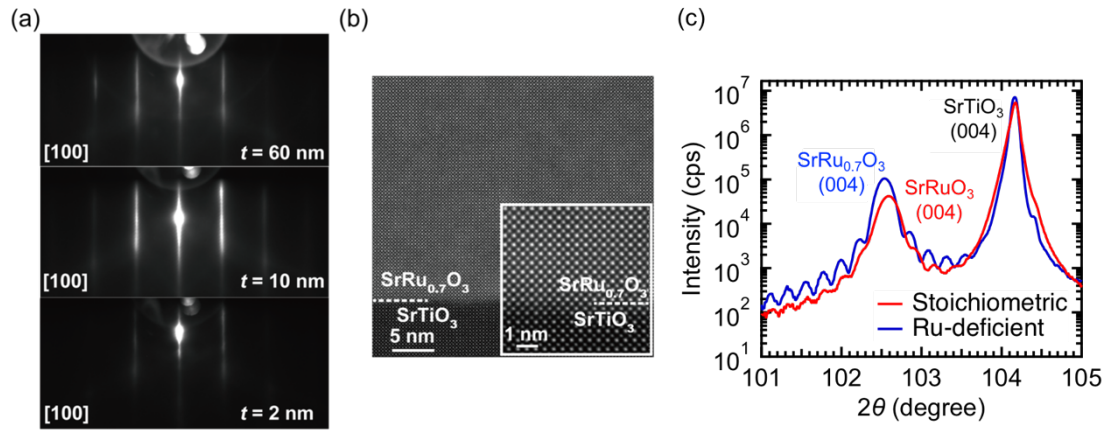


FIG. 2. (a) RHEED patterns of the Ru-deficient $\text{SrRu}_{0.7}\text{O}_3$ films with $t = 60, 10$ and 2 nm taken along the $[100]$ axis of the SrTiO_3 substrates. (b) HAADF-STEM images of the Ru-deficient $\text{SrRu}_{0.7}\text{O}_3$ films taken along the $[100]$ axis of the SrTiO_3 substrates. The inset in (b) is the magnified image near the interface. (c) Comparison of X-ray diffraction patterns between the $\text{SrRu}_{0.7}\text{O}_3$ and SrRuO_3 thin films with $t = 60$ nm.

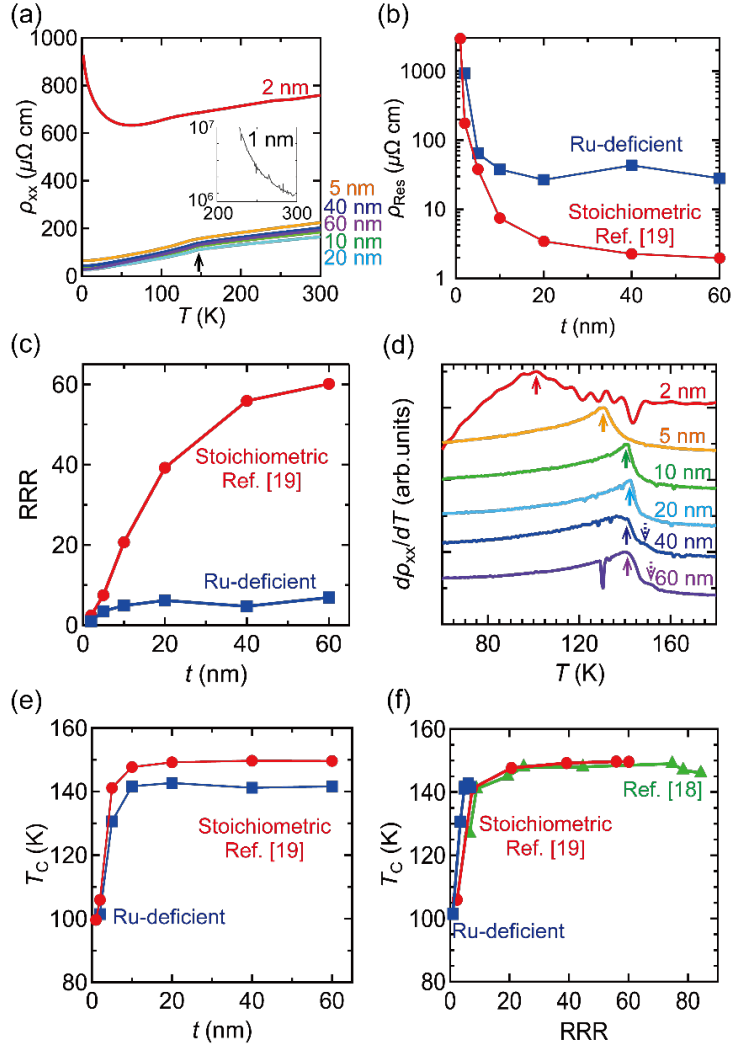


FIG. 3. (a) Temperature dependence of the resistivity ρ_{xx} of the Ru-deficient SrRu_{0.7}O₃ films with various thicknesses t ($=1$ – 60 nm). The arrow indicates the kinks. The inset in (a) shows the data for $t = 1$ nm. (b) Thickness t dependence of the residual resistivity ρ_{Res} of the Ru-deficient SrRu_{0.7}O₃ films. (c) Thickness t dependence of the RRR. The data for the stoichiometric SrRuO₃ films reported in Ref. [19] are also plotted. (d) Temperature dependence of the differential resistivity $d\rho_{xx}/dT$ of the Ru-deficient SrRu_{0.7}O₃ films for various t ($=2$ – 60 nm). Arrows indicate the peak or kink positions in the $d\rho_{xx}/dT$ curves. Dashed arrows indicate shoulder structures. In (d), the $d\rho_{xx}/dT$ has been offset for easy viewing. (e) Thickness t dependence of the T_C obtained from the peak positions of the differential resistivity $d\rho_{xx}/dT$ in (d). The data for the stoichiometric SrRuO₃ films reported in Ref. [19] are also plotted. (f) RRR dependence of the T_C of the Ru-deficient SrRu_{0.7}O₃ films. The data reported in Refs. [18] and [19] are also plotted.

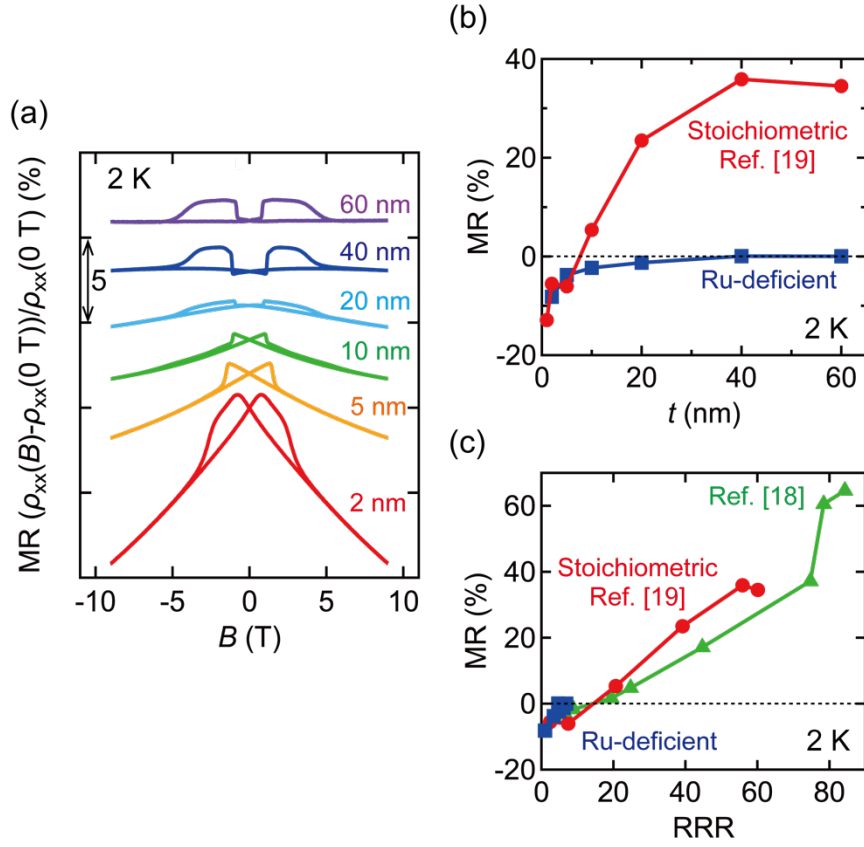


FIG. 4. (a) Thickness t dependence of MR $(\rho_{xx}(B) - \rho_{xx}(0 \text{ T})) / \rho_{xx}(0 \text{ T})$ of the Ru-deficient $\text{SrRu}_{0.7}\text{O}_3$ films at 2 K with B applied in the out-of-plane [001] direction of the SrTiO_3 substrate. (b), (c) Thickness t (b) and RRR (c) dependence of the MR ratio at 2 K with $B = 9 \text{ T}$ applied in the out-of-plane [001] direction of the SrTiO_3 substrate.